

CYCLIC TRANSIT PROBABILITIES OF LONG-PERIOD ECCENTRIC PLANETS DUE TO PERIASTRON PRESSION

STEPHEN R. KANE¹, JONATHAN HORNER², KASPAR VON BRAUN¹

Submitted for publication in the Astrophysical Journal

ABSTRACT

The observed properties of transiting exoplanets are an exceptionally rich source of information that allows us to understand and characterize their physical properties. Unfortunately, only a relatively small fraction of the known exoplanets discovered using the radial velocity technique are known to transit their host, due to the stringent orbital geometry requirements. For each target, the transit probability and predicted transit time can be calculated to great accuracy with refinement of the orbital parameters. However, the transit probability of short period and eccentric orbits can have a reasonable time dependence due to the effects of apsidal and nodal precession, thus altering their transit potential and predicted transit time. Here we investigate the magnitude of these precession effects on transit probabilities and apply this to the known radial velocity exoplanets. We assess the refinement of orbital parameters as a path to measuring these precessions and cyclic transit probabilities.

Subject headings: planetary systems – celestial mechanics – ephemerides – techniques: photometric

1. INTRODUCTION

The realization that we have crossed a technology threshold that allows transiting planets to be detected sparked a flurry of activity in this direction after the historic detection of HD 209458 b's transits (Charbonneau et al. 2000; Henry et al. 2000). This has resulted in an enormous expansion of exoplanetary science such that we can now explore the mass-radius relationship (Burrows et al. 2007; Fortney et al. 2007; Seager et al. 2007) and atmospheres (Agol et al. 2010; Deming et al. 2007a; Knutson et al. 2009a,b) of planets outside of our Solar System. Most of the known transiting planets were discovered using the transit method, but some were later found to transit after first being detected using the radial velocity technique. Two notable examples are HD 17156 b (Barbieri et al. 2007) and HD 80606 b (Laughlin et al. 2009), both of which are in particularly eccentric orbits. Other radial velocity planets are being followed up at predicted transit times (Kane et al. 2009) by the Transit Ephemeris Refinement and Monitoring Survey (TERMS).

Planets in eccentric orbits are particularly interesting because of their enhanced transit probabilities (Kane & von Braun 2008, 2009). This orbital eccentricity also makes those planets prone to orbital precession. In celestial mechanics, there are several kinds of precession which can affect the orbital properties, spin rotation, and equatorial plane of a planet. These have been studied in detail in reference to known transiting planets, particularly in the context of the precession effects on transit times and duration (Carter & Winn 2010; Damiani & Lanza 2011; Heyl & Gladman 2007; Jordán & Bakos 2008; Miralda-Escudé 2002; Pál & Kocsis 2008; Ragozzine & Wolf 2009). One

consequence of these precession effects is that a planet that exhibits visible transits now may not do so at a different epoch and vice versa.

Here we present a study of some precession effects on known exoplanets. The aspect which sets this apart from previous studies is that we are primarily interested in planets not currently known to transit, particularly long-period eccentric planets which have enhanced transit probabilities and larger precession effects. We investigate the subsequent rate of change of the transit probability to show how they drift in and out of a transiting orientation. We calculate the timescales and rates of change for the precession and subsequent transit probabilities and discuss implications for the timescales on which radial velocity planets will enter into a transiting configuration, based upon assumptions regarding their orbital inclinations. We finally compare periastron argument uncertainties to the expected precession timescales and suggest orbital refinement as a means to measure this effect.

2. TRANSIT PROBABILITY

Here we briefly describe the fundamentals of the geometric transit probability for both circular and eccentric orbits. For a detailed description we refer the reader to Kane & von Braun (2008).

In the case of a circular orbit, the geometric transit probability is defined as follows

$$P_t = \frac{R_p + R_\star}{a} \quad (1)$$

where a is the semi-major axis and R_p and R_\star are the radii of the planet and host star respectively. More generally, both the transit and eclipse probabilities are inversely proportional to the star-planet separation where the planet passes the star-observer plane that is perpendicular to the plane of the planetary orbit. The star-planet separation as a function of orbital eccentricity e

skane@ipac.caltech.edu

¹ NASA Exoplanet Science Institute, Caltech, MS 100-22, 770 South Wilson Avenue, Pasadena, CA 91125

² Department of Astrophysics & Optics, School of Physics, University of New South Wales, Sydney, 2052, Australia

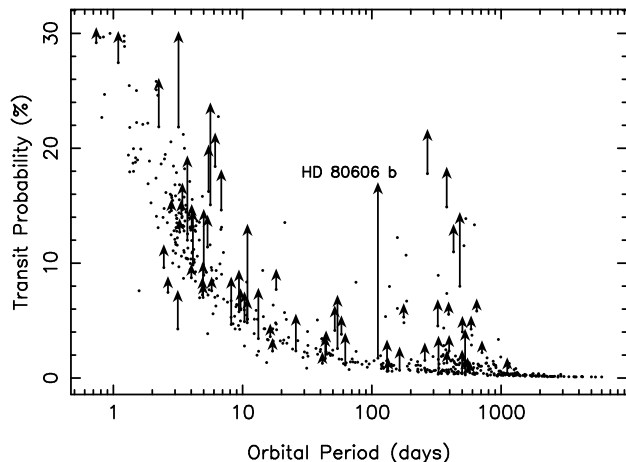


FIG. 1.— Transit probability for a sample of the known exoplanets as a function of orbital period. In cases where a change in ω from current to 90° results in a transit probability improvement $> 1\%$, a vertical arrow indicates the improvement.

is given by

$$r = \frac{a(1 - e^2)}{1 + e \cos f}. \quad (2)$$

where f is the true anomaly, which describes the location of the planet in its orbit, and so is a time dependent variable as the planet orbits the star. For a transit event to occur the condition of $\omega + f = \pi/2$ must be fulfilled (Kane 2007), where ω is the argument of periastron, and so we evaluate the above equations with this condition in place. The geometric transit probability may thus be re-expressed as

$$P_t = \frac{(R_p + R_\star)(1 + e \cos(\pi/2 - \omega))}{a(1 - e^2)} \quad (3)$$

which is valid for any orbital eccentricity. Note that these equations are independent of the true inclination of the planet's orbital plane.

Given the sensitivity of transit probability to the argument of periastron, it is useful to assess how the probabilities for the known exoplanets would alter if their orientation was that most favorable for transit detection: $\omega = 90^\circ$. We extracted data from the Exoplanet Data Explorer³ (Wright et al. 2011) which include the orbital parameters and host star properties for 592 planets and are current as of 30th June 2012. For each planet, we calculate transit probabilities for two cases: (1) using the current value of ω , and (2) using $\omega = 90^\circ$. The transit probabilities for case (1) are shown in Figure 1. Those planets whose case (2) probabilities are improved by $> 1\%$ are indicated by a vertical arrow to the improved probability. There are several features of note in this figure. The relatively high transit probabilities between 100 and 1000 days are due to giant host stars whose large radii dominates the probabilities (see Equation 3)). There are several cases of substantially improved transit probability, most particularly HD 80606 b, which is labelled in the figure. The following sections investigate the periastron precession required to produce such an increase in transit probability.

³ <http://exoplanets.org/>

3. AMPLITUDE OF PERIASTRON (APSIDAL) PRECESSION

Periastron (or apsidal) precession is the gradual rotation of the major axis which joins the orbital apses within the orbital plane. The result of this precession is that the argument of periastron becomes a time dependent quantity. There are a variety of factors which can lead to periastron precession, such as general relativity (GR), stellar quadrupole moments, mutual star-planet tidal deformations, and perturbations from other planets (Jordán & Bakos 2008). For Mercury, the perihelion precession rate due to general relativistic effects is $43''/\text{century}$ ($0.0119^\circ/\text{century}$). By comparison, the precession due to perturbations from the other Solar System planets is $532''/\text{century}$ ($0.148^\circ/\text{century}$) while the oblateness of the Sun (quadrupole moment) causes a negligible contribution of $0.025''/\text{century}$ ($0.000007^\circ/\text{century}$) (Clemence 1947; Iorio 2005).

Here we adopt the formalism of Jordán & Bakos (2008) in evaluating the amplitude of the periastron precession. We first define the orbital angular frequency as

$$n \equiv \sqrt{\frac{GM_\star}{a^3}} = \frac{2\pi}{P} \quad (4)$$

where G is the gravitational constant, M_\star is the mass of the host star, and P is the orbital period of the planet. The total periastron precession is the sum of the individual effects as follows

$$\dot{\omega}_{\text{total}} = \dot{\omega}_{\text{GR}} + \dot{\omega}_{\text{quad}} + \dot{\omega}_{\text{tide}} + \dot{\omega}_{\text{pert}} \quad (5)$$

where the precession components consist of the precession due to GR, stellar quadrupole moment, tidal deformations, and planetary perturbations respectively. Jordán & Bakos (2008) conveniently express these components in units of degrees per century. The components of $\dot{\omega}_{\text{quad}}$ and $\dot{\omega}_{\text{tide}}$ have a^{-2} and a^{-5} dependencies respectively. Since we are mostly concerned with long-period planets in single-planet systems, we consider here only the precession due to general relativity since this is the dominant component in such cases. This imposes a lower limit on the total precession of the system, particularly for multi-planet systems. This precession is given by the following equation

$$\dot{\omega}_{\text{GR}} = \frac{7.78}{(1 - e^2)} \left(\frac{M_\star}{M_\odot}\right) \left(\frac{a}{0.05 \text{ AU}}\right)^{-1} \left(\frac{P}{\text{day}}\right)^{-1} \quad (6)$$

with units in degrees per century.

To examine this precession effect for the known exoplanets, we use the data extracted from the Exoplanet Data Explorer, described in Section 2. The GR precession rates for these planets are shown in Figure 2 as a function of eccentricity, where the radius of the point for each planet is logarithmically scaled with the orbital period. As a Solar System example, the precession rate for Mercury is shown using the appropriate symbol. There are two distinct populations apparent in Figure 2 for which the divide occurs at a periastron precession of $\sim 0.1^\circ/\text{century}$. It is no coincidence that this divide corresponds to the known relative dearth of planets in the semi-major axis range of 0.1–0.6 AU (Burkert & Ida 2007; Cumming et al. 2008; Currie 2009).

As expected from Equation 6, the amplitude of the precession is dominated by the orbital period rather than

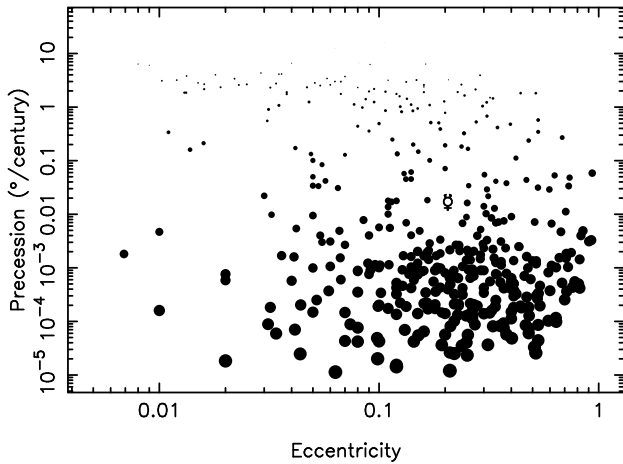


FIG. 2.— Calculated GR periastron precession rates plotted as a function of eccentricity for the known exoplanets with Keplerian orbital solutions. The radius of the points is logarithmically proportional to the orbital period of the planet. The symbol for Mercury is used to indicate its position on the plot.

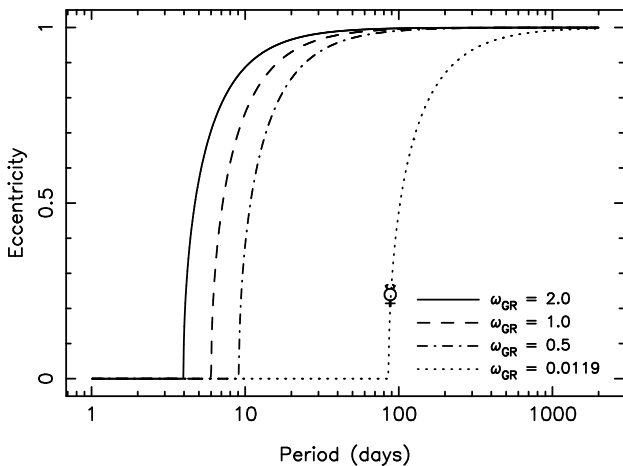


FIG. 3.— Lines of constant GR periastron precession as a function of orbital period and eccentricity, assuming a solar-mass host star. The eccentricity of the orbit only plays a significant role at very large values ($e > 0.8$). The symbol for Mercury is used to indicate its position on the plot.

the orbital eccentricity. Thus, even planets in eccentric orbits do not exhibit significant GR precession at longer periods. This is further demonstrated in Figure 3 where we show lines of constant precession as a function of period and eccentricity for a solar-mass host star. This shows that the GR periastron precession is almost independent of orbital eccentricity except at extreme values of $e > 0.8$. Once again, the location of Mercury on the plot is indicated using the appropriate symbol.

As noted by Miralda-Escudé (2002) and Jordán & Bakos (2008), the total precession time scales are large. Thus what really matters is the rate of change of the periastron argument and quantifying when it is worth returning to a particular target for re-investigation. This is the context of our analysis in Section 4.

3.1. Nodal (Orbital Plane) Precession

For completeness, we briefly consider the effects of nodal precession. Nodal precession occurs when the orbital plane precesses around the total angular momentum

vector, which is usually aligned with the rotation axis of the host star. The precession is caused by the oblateness of the star which results in a non-zero gravitational quadrupole field. This has the potential to be the dominant source of precession when the orbit is polar. For example, the nodal precession for the near-polar retrograde orbit of WASP-33 b has been calculated by Iorio (2011) to be 9×10^9 times larger than that induced on the orbit of Mercury by the oblateness of the Sun.

A description of nodal precession and its effect on transit durations has been provided by Miralda-Escudé (2002). The frequency of nodal precession can be expressed as

$$\Omega = n \frac{R_*^2}{a^2} \frac{3J_2}{4} \sin 2i \quad (7)$$

where n is the orbital angular frequency described in Equation 4, J_2 is the quadrupole moment, and i is the orbital inclination relative to the stellar equatorial plane. A typical quadrupole moment for the star may be approximated as $J_2 \sim 10^{-6}$ and one may expect a relatively aligned orbit such that $\sin 2i \sim 0.1$. For a typical hot Jupiter, values for a are $10R_*$, whereas for Mercury $a = 83R_*$. Since the nodal precession is in units of the orbital angular frequency, one can see that the resulting precession rate is typically several orders of magnitude smaller than that of a hot Jupiter, even at the orbital distance of Mercury. This effect is generally only considered for circular orbits, most notably for short-period orbits that are the most frequently encountered nature of known transiting planets. Here, we are considering longer period eccentric orbits where this is a much smaller effect on the orbital dynamics of the planet.

4. CYCLIC TRANSIT EFFECTS

As discussed in Section 2, the transit probability for a given planet is a function of the periastron argument for orbits with non-zero eccentricity (Kane & von Braun 2008). The precession of the periastron argument thus leads to a cyclic change in the transit probability. Here we quantify this cyclic behaviour and determine rates of change and total timescales.

Using the periastron precession rates calculated in Section 3 and combining these with the transit probability equations of Section 2 allows us to compute the time dependent transit probability for each planet. Recall also that this cyclic behaviour will only occur for planets which have non-zero eccentricities. Shown in Figure 4 are three examples of this time dependence over a period of 100,000 years. When viewing such a plot one is tempted to interpret the cyclic variability in terms of the orbital period, however this variation is caused by the periastron precession, not the orbital period. There is, of course, some period dependency involved, in that shorter period orbits will tend to have a higher cyclic frequency. The planets shown here (HD 88133 b, HD 108147 b, and HD 190360 c) have orbital periods of 3.4, 10.9, and 17.1 days respectively (Butler et al. 2006; Wright et al. 2009). HD 108147 b, in particular, displays very large amplitude variations due to the relatively high eccentricity of its orbit ($e = 0.53$). HD 190360 c has a smaller eccentricity and periastron precession rate, which leads to a cyclic timescale much greater than 100,000 years.

We have performed these calculations for a subset of

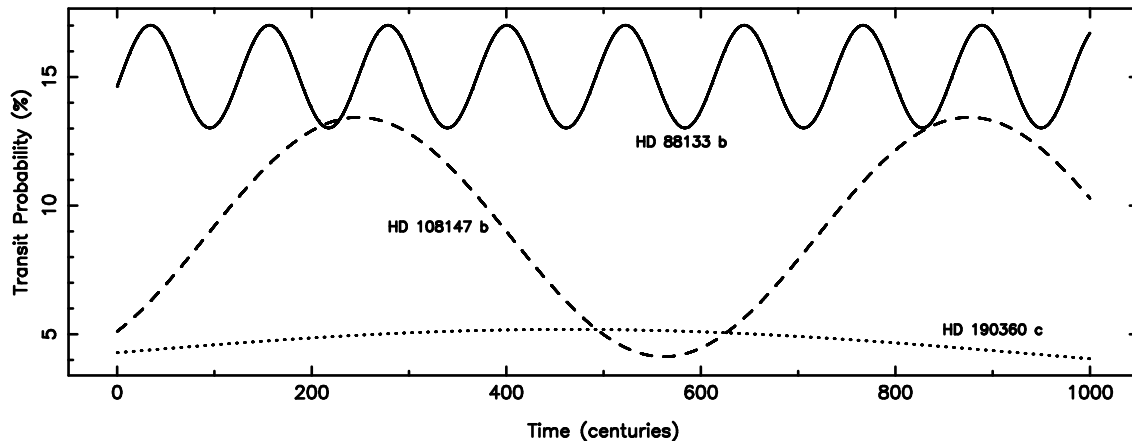


FIG. 4.— Cyclic transit probabilities resulting from GR periastron precession for three known exoplanets: HD 88133 b, HD 108147 b, and HD 190360 c. This is shown from the present epoch and projected 100,000 years from now.

the known exoplanets using the data extracted from the Exoplanet Data Explorer, described in Section 2. We restrict our sample to those planets which are not known to transit and have non-zero eccentricities. The results of these calculations are shown in Table 1 for 60 of the planets. The calculated values include the periastron precession rate ($\dot{\omega}_{\text{GR}}$), transit probability (P_t), maximum transit probability at $\omega = 90^\circ$ (P'_t), time from the current epoch until maximum transit probability (Δt), and the transit probability rate of change (dP_t/dt). The table has been sorted according to dP_t/dt which is presented in units of $\%/century$. The dP_t/dt values have been calculated from the current epoch over the coming century and thus represents the present rate of change. The importance of this is that dP_t/dt is not constant and indeed can have negative values as the periastron argument rotates past $\omega = 90^\circ$. Specifically, dP_t/dt will be negative for $90^\circ < \omega < 270^\circ$ and positive elsewhere. This further restricts the planets considered to those whose current ω falls in this range such that $dP_t/dt > 0$.

It can be clearly seen that the time required to reach maximum transit probability is immense, certainly beyond the lifetime of anyone reading this work. However, the rate of change can yield an improved idea of which planets may have a measurable change in configuration. Consider the case of HD 156846 b, whose orbital parameters and transit potential have been studied in detail by Kane et al. (2011). This is one of the planets in the table with the longest period and also has one of the highest orbital eccentricities. The transit probability is relatively high for this planet and is close to the maximum probability since ω only needs to change by 38° . Even so, observations of the periastron precession are unlikely for the timescales involved. By contrast, the hot Saturn HD 88133 b discovered by Fischer et al. (2005) has the highest transit probability rate of change.

5. CONCLUSIONS

Transiting planets have become an essential component of exoplanetary science due to the exceptional opportunities they present for characterization of these planets. Many of the known exoplanets discovered through the radial velocity technique are currently not known to transit. However, transit probabilities can be substantially improved if the periastron argument ap-

proaches $\omega = 90^\circ$. Since, for eccentric orbits, the periastron argument is time dependent as a result of their precession, planets which do not transit at the present epoch may transit in the future and vice versa. The planet Mercury falls quite central to the current distribution of calculated periastron precessions for the known exoplanets. This distribution has an eccentricity dependence but is most strongly affected by the orbital period. If a precession rate for a given planet is found to be markedly different from our calculations then this could be indicative of further, as yet undiscovered planets in that system. These additional planets would normally be detected from the radial velocity data unless insufficient observations allow them to remain hidden.

The periastron precession leads to a cyclic transit probability variation for all exoplanets with non-zero eccentricities. Timescales vary enormously but will likely lead to many of these planets transiting their host stars at some point in the future. A reasonable question to ask at this point is if the periastron arguments of the known planets are known with sufficient precision to detect precession in any acceptable timeframe. Once again, we exploit the data extracted from the Exoplanet Data Explorer, described in Section 2. The uncertainties associated with the values of ω for all these planets have a mean of 28° and a median of 15° . This is much higher than the precession effects shown in Table 1. A program of refining the orbits of the known exoplanets, such as that described by Kane et al. (2009), would result in many of these precession effects to be detectable in reasonable time frames. For example the first planet in the table, HD 88133 b, has a precession rate that will cause a shift of $\sim 0.3^\circ$ per decade. Uncertainties on ω of less than one degree are not unusual and can certainly be achieved for those planets in particularly eccentric orbits. The exoplanet HD 156846 b has a current ω uncertainty of 0.16° (Kane et al. 2011) which demonstrates that such refinement is possible even for relatively long-period planets. More data and longer time baselines will produce subsequent improvements for many more planets which can result in the detection of the precession for high-precession cases.

The relevance of this work may be extended to the Kepler mission which has detected many candidate multi-planet systems (Borucki et al. 2011a,b; Batalha et al.

TABLE 1
EXOPLANET PERIASTRON PRECESSION, TRANSIT PROBABILITIES, AND TIMESCALES

Planet	P (days)	e	ω	$\dot{\omega}_{GR}$ ($^{\circ}/\text{cent}$)	P_t (%)	P'_t (%) ¹	Δt (cent) ²	dP_t/dt (%/cent) ³
HD 88133 b	3.42	0.13	349.0	2.9490	14.6	17.0	34.2	0.101368
HD 76700 b	3.97	0.09	30.0	2.1838	12.9	13.5	27.5	0.038099
HD 73256 b	2.55	0.03	337.3	4.3194	16.1	16.8	26.1	0.033421
HD 108147 b	10.90	0.53	308.0	0.5732	5.1	13.4	247.7	0.028841
HD 102956 b	6.49	0.05	12.0	1.2451	22.8	23.6	62.6	0.022932
BD -08 2823 b	5.60	0.15	30.0	0.9420	11.6	12.4	63.7	0.022925
HD 7924 b	5.40	0.17	25.0	1.0901	7.2	7.9	59.6	0.019663
HD 68988 b	6.28	0.12	31.4	1.0214	8.7	9.1	57.4	0.015372
HD 1461 b	5.77	0.14	58.0	1.1102	9.4	9.6	28.8	0.011871
HD 217107 b	7.13	0.13	24.4	0.8192	6.9	7.4	80.1	0.010737
HD 168746 b	6.40	0.11	17.0	0.8587	7.2	7.7	85.0	0.010620
HD 149143 b	4.07	0.02	0.0	2.1614	15.5	15.8	41.6	0.009380
HD 162020 b	8.43	0.28	28.4	0.5283	4.7	5.3	116.6	0.009352
HD 187123 b	3.10	0.01	24.5	3.0953	13.5	13.6	21.1	0.006702
HD 47186 b	4.08	0.04	59.0	1.8945	11.0	11.0	16.4	0.006690
BD -10 3166 b	3.49	0.02	334.0	2.3445	8.7	8.9	49.5	0.006174
HD 69830 b	8.67	0.10	340.0	0.4923	5.4	6.1	223.5	0.004500
HD 190360 c	17.11	0.24	5.2	0.1833	4.3	5.2	462.8	0.003171
upsilon And b	4.62	0.01	51.0	1.8588	12.0	12.0	21.0	0.003147
HD 179079 b	14.48	0.12	357.0	0.2481	5.3	6.0	374.8	0.002675
51 Peg b	4.23	0.01	58.0	1.8602	10.1	10.1	17.2	0.002169
HD 10180 c	5.76	0.08	279.0	1.1232	7.6	8.8	152.2	0.002059
HIP 57274 b	8.14	0.19	81.0	0.5075	5.3	5.3	17.7	0.001124
HD 147018 b	44.24	0.47	336.0	0.0437	2.3	4.1	2607.5	0.000922
HD 16417 b	17.24	0.20	77.0	0.1935	6.3	6.4	67.2	0.000801
HD 10180 d	16.36	0.14	292.0	0.2001	3.6	4.7	789.4	0.000780
HD 163607 b	75.29	0.73	78.7	0.0336	8.3	8.4	336.7	0.000406
HD 224693 b	26.73	0.05	6.0	0.1008	3.2	3.4	833.1	0.000283
4 UMa b	269.30	0.43	23.8	0.0025	17.8	21.7	26488.3	0.000263
61 Vir c	38.02	0.14	341.0	0.0453	2.1	2.5	2405.3	0.000227
HD 102117 b	20.81	0.12	279.0	0.1351	3.3	4.2	1266.0	0.000169
HD 43691 b	36.96	0.14	290.0	0.0612	2.6	3.4	2612.5	0.000152
70 Vir b	116.69	0.40	358.7	0.0090	1.9	2.7	10097.0	0.000124
HD 156846 b	359.51	0.85	52.2	0.0049	4.4	4.8	7699.5	0.000116
HD 16141 b	75.52	0.25	42.0	0.0163	2.3	2.5	2950.5	0.000105
GJ 785 b	74.39	0.30	15.0	0.0141	1.4	1.6	5332.1	0.000089
HIP 57274 c	32.03	0.05	356.2	0.0500	1.9	2.0	1876.0	0.000083
HD 4113 b	526.62	0.90	317.7	0.0031	0.9	4.3	42500.7	0.000082
rho CrB b	39.84	0.06	303.0	0.0419	2.3	2.6	3510.1	0.000055
HD 45652 b	43.60	0.38	273.0	0.0380	1.7	3.8	4660.2	0.000036
HD 20868 b	380.85	0.75	356.2	0.0019	1.3	2.4	48796.3	0.000035
61 Vir d	123.01	0.35	314.0	0.0072	0.8	1.5	19010.2	0.000034
55 Cnc c	44.38	0.05	57.4	0.0335	2.1	2.1	972.3	0.000033
HD 60532 b	201.30	0.28	351.9	0.0040	1.6	2.1	24667.9	0.000032
HD 145457 b	176.30	0.11	300.0	0.0056	5.3	6.5	26940.2	0.000032
GJ 581 d	66.64	0.25	356.0	0.0089	0.7	0.9	10602.7	0.000029
HD 5891 b	177.11	0.07	351.0	0.0049	4.8	5.2	20191.3	0.000027
HD 1237 b	133.71	0.51	290.7	0.0072	0.6	1.8	22236.9	0.000027
HD 17092 b	359.90	0.17	347.4	0.0020	2.8	3.4	52495.0	0.000016
HD 22781 b	528.07	0.82	315.9	0.0014	0.4	1.8	93315.9	0.000015
HD 107148 b	48.06	0.05	75.0	0.0342	2.1	2.1	439.0	0.000015
BD +48 738 b	392.60	0.20	358.9	0.0008	5.5	6.7	113252.5	0.000015
HD 180314 b	396.03	0.26	303.1	0.0019	2.3	3.8	78180.5	0.000014
HIP 14810 c	147.77	0.15	327.3	0.0049	1.1	1.4	25078.6	0.000013
HD 8574 b	227.00	0.30	26.6	0.0028	1.1	1.3	22763.8	0.000013
HD 216770 b	118.45	0.37	281.0	0.0075	0.8	1.8	22495.8	0.000012
HD 93083 b	143.58	0.14	333.5	0.0041	1.1	1.3	28700.1	0.000010
HD 11977 b	711.00	0.40	351.5	0.0006	2.2	3.3	153321.8	0.000010
HD 222582 b	572.38	0.73	319.0	0.0010	0.5	1.5	126637.2	0.000009
HD 231701 b	141.60	0.10	46.0	0.0057	1.2	1.2	7727.6	0.000008

¹ P'_t refers to the transit probability where $\omega = 90^{\circ}$.

² Δt refers to the time until P'_t occurs.

³ dP_t/dt is calculated over the coming century but is a time dependent quantity.

2012), most of which are likely to be real exoplanets (Lissauer et al. 2012). Due to simply geometric transit probabilities, most of these systems will certainly have planets which are not transiting the host star at present. The known transiting multi-planet systems are largely in circular orbits, but may have periastron precession due to perturbations from other planets leading to an eventual transit from currently non-transiting planets in the system. For example, Kepler-19 c is known to exist from Transit Timing Variations of the inner planet, but does not currently have a detectable transit signature. Similarly, some of these planets will cease exhibiting an observable transit signature. Issues such as these are important for considering the completeness of these surveys in determining multi-planetary system architectures.

ACKNOWLEDGEMENTS

The authors would like to thank David Ciardi and Solange Ramirez for several useful discussions and the numerous people who have requested that we perform this study. We would also like to thank the anonymous referee, whose comments greatly improved the quality of the paper. JH gratefully acknowledges the financial support of the Australian government through ARC Grant DP0774000. This research has made use of the Exoplanet Orbit Database and the Exoplanet Data Explorer at exoplanets.org. This research has also made use of the NASA Exoplanet Archive, which is operated by the California Institute of Technology, under contract with the National Aeronautics and Space Administration under the Exoplanet Exploration Program.

REFERENCES

- Agol, E., Cowan, N.B., Knutson, H.A., Deming, D., Steffan, J.H., Henry, G.W., Charbonneau, D. 2010, *ApJ*, 721, 1861
 Barbieri, M., et al. 2007, *A&A*, 476, L13
 Batalha, N.M., et al. 2012, *ApJS*, submitted (arXiv:1202.5852)
 Borucki, W.J., et al. 2011, *ApJ*, 728, 117
 Borucki, W.J., et al. 2011, *ApJ*, 736, 19
 Burrows, A., Hubeny, I., Budaj, J., Hubbard, W.B. 2007, *ApJ*, 661, 502
 Burkert, A., Ida, S. 2007, *ApJ*, 660, 845
 Butler, R.P. et al. 2006, *ApJ*, 646, 505
 Carter, J.A., Winn, J.N. 2010, *ApJ*, 716, 850
 Charbonneau, D., Brown, T.M., Latham, D.W., Mayor, M., 2000, *ApJ*, 529, L45
 Clemence, G.M. 1947, *RvMP*, 19, 361
 Cumming, A., Butler, R.P., Marcy, G.W., Vogt, S.S., Wright, J.T., Fischer, D.A. 2008, *PASP*, 120, 531
 Currie, T. 2009, *ApJ*, 694, L171
 Damiani, C., Lanza, A.F. 2011, *A&A*, 535, 116
 Deming, D., Richardson, L.J., Harrington, J. 2007, *MNRAS*, 378, 148
 Fischer, D.A., et al. 2005, *ApJ*, 620, 481
 Fortney, J.J., Marley, M.S., Barnes, J.W., 2007, *ApJ*, 659, 1661
 Henry, G.W., Marcy, G.W., Butler, R.P., Vogt, S.S., 2000, *ApJ*, 529, L41
 Heyl, J.S., Gladman, B.J. 2007, *MNRAS*, 377, 1511
 Iorio, L. 2005, *A&A*, 433, 385
 Iorio, L. 2011, *Ap&SS*, 331, 485
 Jordán, A., Bakos, G.A. 2008, *ApJ*, 685, 543
 Kane, S.R. 2007, *MNRAS*, 380, 1488
 Kane, S.R., von Braun, K. 2008, *ApJ*, 689, 492
 Kane, S.R., von Braun, K., 2009, *PASP*, 121, 1096
 Kane, S.R., Mahadevan, S., von Braun, K., Laughlin, G., Ciardi, D.R. 2009, *PASP*, 121, 1386
 Kane, S.R., et al. 2011, *ApJ*, 733, 28
 Knutson, H.A., et al. 2009a, *ApJ*, 690, 822
 Knutson, H.A., Charbonneau, D., Cowan, N.B., Fortney, J.J., Showman, A.P., Agol, E., Henry, G.W. 2009b, *ApJ*, 703, 769
 Laughlin, G., Deming, D., Langton, J., Kasen, D., Vogt, S., Butler, P., Rivera, E., Meschiari, S. 2009, *Nature*, 457, 562
 Lissauer, J.J., et al. 2012, *ApJ*, 750, 112
 Miralda-Escudé, J. 2002, *ApJ*, 564, 1019
 Pál, A., Kocsis, B. 2008, *MNRAS*, 389, 191
 Ragozzine, D., Wolf, A.S. 2009, *ApJ*, 698, 1778
 Seager, S., Kuchner, M., Hier-Majumder, C.A., Militzer, B. 2007, *ApJ*, 669, 1279
 Wright, J.T., Upadhyay, S., Marcy, G.W., Fischer, D.A., Ford, E.B., Johnson, J.A. 2009, *ApJ*, 693, 1084
 Wright, J.T., et al., 2011, *PASP*, 123, 412